RSC Advances

PAPER

View Article Online
View Journal | View Issue

Cite this: *RSC Adv.*, 2021, **11**, 4318

Palladium supported on mixed-metal–organic framework (Co–Mn-MOF-74) for efficient catalytic oxidation of CO†

Reda S. Salama, *[a] Mohammed A. Mannaa, [b] Hatem M. Altass,[c] Amr Awad Ibrahim [d] and Abd El-Rahman S. Khder *[cd]

Successful monometallic and bimetallic metal–organic frameworks with different Co/Mn ratios have been synthesized under solvothermal conditions. The as-synthesized MOFs followed by deposition of Pd nanoparticles with 0.5 to 7 wt%. The XRD, BET, SEM, TEM, EDAX and FT-IR characterization results reveal that bimetallic MOFs and Pd nanoparticles were finely dispersed on the prepared MOFs surfaces. XRD results confirm the formation of the desire MOFs and show the high degree of dispersion of Pd nanoparticles. TEM images show that Pd nanoparticles are nano-sized with almost uniform shape. EDAX shows that Pd nanoparticles successfully loaded on $Co_{0.5}$–$Mn_{0.5}$-MOF-74 catalyst. CO oxidation as a model reaction was then used to assess the catalytic performance of the prepared catalysts. The catalytic activity results show enhancement in the catalytic activities of monometallic MOFs after introducing another metal in the same framework and show an excellent improvement in CO conversion after loading with Pd nanoparticles. Furthermore, the samples that contain Pd nanoparticles exhibits higher catalytic activities which raised with increasing the content of Pd nanoparticles.

Received 24th November 2020
Accepted 24th December 2020

DOI: 10.1039/d0ra09970h

rsc.li/rsc-advances

1. Introduction

Metal–organic frameworks (MOFs) are a new class of porous coordination polymers, which are constructed from chemical interaction between metal ions or clusters and organic linkers.[1] MOFs attracted much attention in the last few years due to its excellent properties such as extremely high surface area, tunable pore sizes, ordered crystalline structures and remarkable permanent porosity.[2–5] MOFs have numerous applications like catalysis,[2] gas storage,[6] drug delivery,[7] separation[3] and in batteries.[8] However, these monometallic MOF-based nanocomposites are not cost-effective, and their synthetic processes are comparatively complex. Therefore, an increasing number of researchers have employed bimetallic MOFs in various fields such as in degradation of toxic compounds,[9] gas conversion,[10] CO oxidation[11] and gas uptake.[12] Bimetallic metal–organic frameworks have improved catalytic performance than monometallic MOFs because of the exclusive properties of bimetallic materials. However, the introduction of bimetallic nodes into the same MOFs can produce defects and remarkable synergistic effects, which may also raise the number of active sites and further improve the catalytic activity.[13]

The active metal sites and/or reactive organic groups that are existed in the frameworks of MOFs provide the catalytic functions of the MOFs. As well as, catalytic metal nanoparticles (NPs) supported into MOFs cavities can also offer catalytic function. Palladium nanoparticles have been extensively useful in numerous applications like sensing,[14,15] catalysis[16–19] and biomedical.[20] So, the synthesis of Pd-NP based catalysts attracted much attention in the last few years. However, palladium NP catalysts also suffer from some persistent difficulties such as oxidation and self-agglomeration that reduces its catalytic activities.[21,22] Thus, it is very important to select a suitable support for palladium NPs to enhance the activity and stability. In earlier literature, the incorporation of metal NPs into porous supports, such as metal–organic frameworks (MOFs), mesoporous materials and zeolites, can be attained by several approaches, including chemical vapor deposition,[23] impregnation method[24,25] and solid grinding.[26] The catalytic activities of numerous modified and unmodified MOF-based catalysts have been examined for liquid-phase reactions such as hydrogenation, isomerization, polymerization and cyanosilylation.[27,28] In contrast to liquid-phase reactions, only a limited gas–solid reactions and gas-phase reactions using MOF-based catalysts

[a]*Basic Science Department, Faculty of Engineering, Delta University for Science and Technology, Gamasa, Egypt. E-mail: reda.salama@deltauniv.edu.eg; dr.reda.salama@gmail.com*

[b]*Chemistry Department, Faculty of Science, Sa'ada University, Yemen. E-mail: mnnaam@yahoo.com*

[c]*Research Laboratories Unit, Chemistry Department, Faculty of Applied Science, Umm Al-Qura University, 21955 Makkah, Saudi Arabia. E-mail: hutass@uqu.edu.sa*

[d]*Chemistry Department, Faculty of Science, Mansoura University, Mansoura, 35516, Egypt. E-mail: amr_awad@mans.edu.eg; askhder2244@yahoo.com*

† Electronic supplementary information (ESI) available. See DOI: 10.1039/d0ra09970h

have been demonstrated. For example, a few researches exist on the use of MOF-based catalysts for CO oxidation.[29–31]

One of the most poisonous gas is carbon monoxide (CO) which has toxic effect on human health at concentration over 35 ppm.[32] CO or carbon monoxide is produced from the partial oxidation or incomplete burning of several fuels such as gasoline, natural gas and coal. It is odorless, colorless but toxic and even deadly gas because of its high affinity to bind hemoglobin in blood cells.[33] Huge amount of carbon monoxide is continuously being released regularly from power plants, transportation and domestic and industrial activities.[34] CO is also the creator of ground-level ozone, which is responsible for numerous respiratory problems. Also, it is not well soluble in water, which also limits its removal from air by means of aqueous treatments. So its oxidation into CO_2 is a key solution for CO reduction in air depollution managements. CO oxidation is one of the most commonly investigated reactions in the field of heterogeneous catalysis which received much attention in the last few years due to its significance in fuel cells, gas sensors, automotive exhaust treatment as well as air purification.[35–37] To attain CO removal, it is necessary to design catalysts, which permits the oxidation reaction with a sufficient rate.

Herein, a series of new bimetallic Co/Mn-MOFs were successfully synthesized *via* a direct solvothermal method. The catalytic activities of as-synthesized bimetallic MOFs were enhanced through addition of different amounts of palladium nanoparticles. The textural and surface chemistry properties of as-synthesized catalysts were analyzed *via* various techniques such as XRD, BET, TEM, SEM, EDAX and FT-IR then linked to their catalytic behaviors in CO oxidations. Furthermore, the stability of the catalysts was also evaluated in successive runs.

2. Experimental

2.1 Materials

2,5-Dihydroxyterphthalic acid (DHTP) [$C_8H_6O_6$, 98%], manganese(II) chloride [$MnCl_2 \cdot 4H_2O$, 99%], cobalt(II) chloride [$CoCl_2 \cdot 6H_2O$, 99%], palladium nitrate [$Pd(NO_3)_2$, 99.995%] and hydrazine hydrate (80% solution in water) were purchased from Sigma-Aldrich. *N*,*N*-Dimethylformamide (DMF) [$(CH_3)_2N$-CHO, ≥99.5%] and Ethanol [C_2H_5OH, ≥99.5%] were obtained from Alfa Aesar. All organic and inorganic chemicals used in the preparation of the catalysts were directly used without further purifications.

2.2 Synthesis of Co/Mn-MOF-74

Monometallic and bimetallic MOF-74 were synthesized according to a previous reported method with some modifications.[13] All the MOF-74 samples were synthesized through solvothermal method using 6 mmol of metal precursor and 1.5 mmol of 2,5-dihydroxyterphthalic acid (DHTP) in 60 ml solvent using hydrothermal method. In order to synthesize cobalt and/or manganese MOF-74, different molar ratios (1 : 0, 0.75 : 0.25, 1 : 1, 0.25 : 0.75 and 0 : 1) of $CoCl_2 \cdot 6H_2O$ and $MnCl_2 \cdot 4H_2O$ with a total 6.0 mmol of metal precursor were used during the preparation process. For example the detailed preparation steps of $Mn_{0.5}$–$Co_{0.5}$-MOF-74 are as follows: $CoCl_2 \cdot 6H_2O$ (3 mmol, 0.357 g) and $MnCl_2 \cdot 4H_2O$ (3 mmol, 0.296 g) were dissolved in 40 ml of ethanol. The 2,5-dihydroxyterphthalic acid (DHTP) was also dissolved in 20 ml DMF. After complete dissolution, the two solutions were mixed together under constant stirring for 10 min and then transferred to a Teflon-lined autoclave (100 ml). The autoclave was heated in isolated oven to 150 °C for 12 h with a heating rate of 3 °C per min. After that, the sample was filtered and washed firstly with DMF for 3 times and then with ethanol for 3 times to remove any impurities or unreacted DHTP. Finally, the sample was dried at 80 °C for 12 h under vacuum.

2.3 Synthesis of Pd@Co/Mn-MOF-74

Palladium nanoparticles supported monometallic and bimetallic MOF-74 (x wt% Pd@(Co-MOF-74 or Mn-MOF-74 or Co_x–$Mn_{(1-x)}$-MOF-74)) catalysts were prepared using microwave-assisted synthesis. Typically, 2 g of previously dried MOF-74 was suspended and sonicated in 25 ml of distilled water. Then the calculated volumes of palladium(II) nitrate solution and 500 μl of hydrazine hydrate were mixed and stirred vigorously for 5 h. Finally, the mixture was transfer to the microwave oven for 2 min for compete the reduction of Pd^{2+} ions.[38–40]

2.4 Catalyst characterization

2.4.1 XRD measurements. The crystallinity of the as-synthesized samples was identified using X'Pert Philips X-ray powder diffractometer using Cu Kα (λ = 0.15417 nm) with voltage and current at 40 kV and 45 mA, respectively. The sample was scanned over the range 7–80° at a scanning rate of 2° min^{-1} to identify the crystalline structure.

2.4.2 BET measurements. The adsorption/desorption isotherms and specific surface area of the as-synthesized catalysts were measured from N_2 adsorption studies conducted at −196 °C using Quantachrom Nova Sorbimetric system. The samples were previously outgassed at 120 °C for 2 h.

2.4.3 FTIR spectroscopic studies. The chemical structure and functional groups of the as-synthesized catalysts were recorded *via* Nicolet-Nexus 670 FT-IR spectrophotometer in the transition mode with dried KBr pellets and a measuring range of 400–2000 cm^{-1}.

2.4.4 SEM and TEM images. The morphology of the catalysts were examined using scanning electron microscope (SEM, Jeol JSM-6510LV). TEM images and particle size were obtained using (TEM, Jeol JEM-1230) operated at 120 kV. Typically, the catalyst was dispersed in methanol using ultrasonic radiation for 10 min then a drop of the suspension was transferred onto carbon-coated copper grids.

2.4.5 Testing the CO oxidation activity. The catalytic oxidation of carbon monoxide by oxygen was performed through the following: 50 mg of the as-synthesized catalyst, treated for 15 min at 110 °C in the He gas flow to eliminate moisture and adsorbed impurities, was transferred inside a tubular quartz reactor with an inner diameter (i.d) equal 6 nm then placed inside Thermolyne 2100 programmable tube furnace reactor. The temperature of the prepared samples was

measured using a thermocouple placed near the sample. Typically, a gas mixture containing 4 wt% CO, 20 wt% O_2 and 76 wt% Ar was passed over the sample with a flow rate equal 50 $cm^3\ min^{-1}$ while the temperature of the catalyst was raised from room temperature till complete oxidation of CO with a heat rate 5 °C min^{-1}. The conversion of CO to CO_2 was observed using an infrared gas analyzer (MGA 3000 multi-gas analyzer, ADC).

3. Results and discussion

3.1 X-ray diffraction pattern (XRD)

The crystal structures of Mn-MOF-74, Co-MOF-74 and $Co_{0.5}$–$Mn_{0.5}$-MOF-74 were investigated using XRD analysis and displayed in Fig. 1. Mn-MOF-74 shows characteristic peaks at 2θ equal 6.9, 7.5, 13.5, 14.2, 15.5, 17.9, 19.3, 24.6, 26.5, 29.7, 31.8, 33.5, 34.5, 43.6, 50.3 and 58.2°. On the other hand, XRD patterns of Co-MOF-74 were recognized at 2θ equal 11.3, 14.5, 16.3, 18.1, 29.2, 31.2, 33.5, 44.9 and 59.8°, which were almost identical to the previously reported XRD pattern of Mn-MOF-74 (ref. 41–43) and Co-MOF-74,[44–46] respectively. The XRD pattern of $Co_{0.5}$–$Mn_{0.5}$-MOF-74 were very similar to those of the monometallic MOF-74 (Mn and Co) samples and there are no new peaks could be observed after insertion the other metal in the same framework which showed that the catalyst still preserves its crystalline structure and indicating that the bimetallic MOF is a single-phase crystal and the inserted metal (Co) was not loaded MOF-74 (Mn) framework. However, the peak with 2θ equal 6.9° observed in XRD pattern of Mn-MOF-74 shifted toward a higher value after mixing with cobalt as shown in Fig. 1 (inset). This may be due to replacing of larger Mn(II) ions with ionic radii 0.97 Å with smaller coordinated Co(II) cations with ionic radii 0.92 Å which resulted in shrinking of the crystal lattice.[47,48] Therefore, it was further proved that two kinds of metals coexisted in the same framework.[49]

The wide-angle powder XRD patterns for 2 wt% of Pd over Co-MOF-74, Mn-MOF-74 and $Co_{0.5}$–$Mn_{0.5}$-MOF-74 were displayed in Fig. 2. The figure displays that the basic structure of the as-synthesized metal–organic frameworks was well

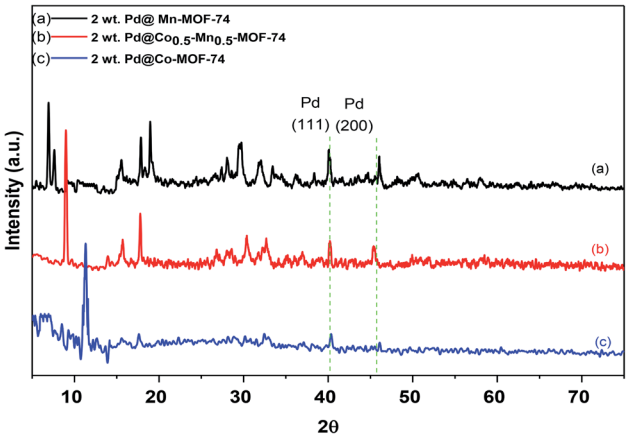

Fig. 2 XRD patterns of 2 wt% Pd NPs loaded on (a) Mn-MOF-74, (b) $Co_{0.5}$–$Mn_{0.5}$-MOF-74 and (c) Co-MOF-74.

maintained after loading 2 wt% of Pd and the good crystallinity was observed through the sharp diffraction peaks. There are some additional Bragg peaks corresponding to Pd nanoparticles were observed in monometallic and bimetallic MOFs at 2θ equal 40.1 and 46.1°, assigned to (111) and (200), respectively.[50] Also, Fig. 2b shows the peaks intensity of $Co_{0.5}$–$Mn_{0.5}$-MOF-74 decreased after loading of Pd nanoparticles indicating that the Pd inhibited the growth the crystallinity of $Co_{0.5}$–$Mn_{0.5}$-MOF-74.

3.2 BET measurements

Fig. 3 displays the nitrogen adsorption isotherms of mixed CoMn-MOFs samples, along with that of pure Co-MOF-74 and Mn-MOF-74 samples. The adsorption and desorption curves display a typical type-II isotherms according to IUPAC[48,51,52] classification with a H3 type hysteresis loop, which is characteristic of the presence of a large proportion of meso and macro porous materials. The specific BET surface areas (S_{BET}) of the as-synthesized MOFs were shown in Table 1. The BET surface area of pure Co-MOF-74 and Mn-MOF-74 are 477.3 and 481.3 $m^2\ g^{-1}$,

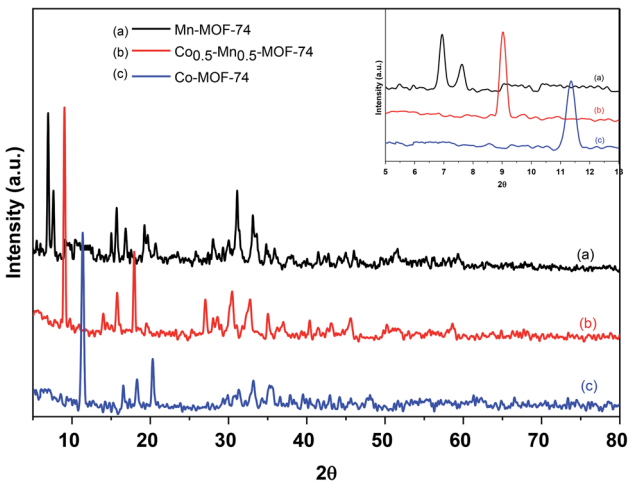

Fig. 1 XRD patterns of monometallic and bimetallic MOF-74.

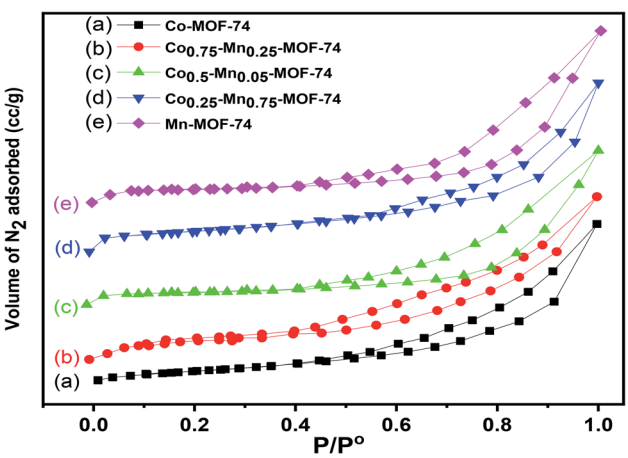

Fig. 3 Adsorption–desorption isotherms of nitrogen at 196 °C on monometallic and bimetallic MOFs.

Table 1 Textural properties and catalytic activity results of the as-synthesized catalysts

Catalyst	S_{BET} (m^2 g^{-1})	Pore volume (cm^3 g^{-1})	Pore radius (Å)	CO conversion	
				T_{50} (50%)	T_{100} (100%)
Mn-MOF-74	481.3	0.419	19.7	527 (44%)	—
$Co_{0.25}$–$Mn_{0.75}$-MOF-74	490.2	0.415	17.4	445	—
$Co_{0.5}$–$Mn_{0.5}$-MOF-74	518.6	0.448	17.0	383	—
$Co_{0.75}$–$Mn_{0.25}$-MOF-74	494.2	0.432	17.3	536	—
Co-MOF-74	477.3	0.428	19.3	490	—
2 wt% Pd@Mn-MOF-74	440.7	0.309	16.9	144	146
2 wt% Pd@$Co_{0.25}$–$Mn_{0.75}$-MOF-74	453.5	0.311	17.1	101	109
2 wt% Pd@$Co_{0.5}$–$Mn_{0.5}$-MOF-74	487.8	0.301	16.7	57	68
2 wt% Pd@$Co_{0.75}$–$Mn_{0.25}$-MOF-74	462.1	0.282	17.0	73	90
2 wt% Pd@Co-MOF-74	434.8	0.246	18.8	135	140
0.05 wt% Pd@$Co_{0.5}$–$Mn_{0.5}$-MOF-74	491.2	0.440	17.1	259	290
5 wt% Pd@$Co_{0.5}$–$Mn_{0.5}$-MOF-74	432.1	0.275	16.4	50	58
7 wt% Pd@$Co_{0.5}$–$Mn_{0.5}$-MOF-74	—	—	—	73	84

respectively. After introducing two metals in the same frameworks, bimetallic CoMn-MOFs have larger specific surface area compared with monometallic Co-MOF-74 and Mn-MOF-74; this suggested that the introduction of two nodes into the same metal–organic frameworks generates more internal defects. Among the as-synthesized bimetallic MOFs, $Co_{0.5}$–$Mn_{0.5}$-MOF-74 displays largest surface area, which may be due to synergetic effect between two metals.[13] After modification by palladium nanoparticles, little difference in the adsorption desorption isotherms could be observed as shown in Fig. 1S,† which means introducing of Pd nanoparticles does not effect on the structure of the as-synthesized MOFs. The Pd loaded on $Co_{0.5}$–$Mn_{0.5}$-MOF-74 samples exhibited a significant decrease in the S_{BET} values with increasing palladium contents to 432.1 m^2 g^{-1} which may be due to deposition of palladium nanoparticles inside the pores of the as-synthesized MOF.

The pore size distributions of pure Co-MOF, Mn-MOF, mixed CoMn-MOFs and Pd loaded on as-synthesized MOFs were determined using Barrett–Joyner–Halenda (BJH) method and the isotherms are presented in Fig. 4. The pore volume of the loaded samples and bimetallic MOFs are much lower compared to that of pure Co-MOF-74 and Mn-MOF-74 as shown in Table 1. The results show a unique peak centered at about 19.3 and 19.7 Å diameters for pure Co-MOF-74 and Mn-MOF-74 while the pore radius of bimetallic MOFs shifted to 17.0 Å. On the other hand, the samples loaded with different amount of Pd nanoparticles show much lower pore radium (16.4 Å) which may be due to the fact that the Pd is deposited inside the pores.

3.3 Fourier transform infrared (FT-IR)

The FT-IR spectra of the prepared samples illustrated that the monometallic (Co-MOF-74 and Mn-MOF-74) and bimetallic MOF ($Co_{0.5}$–$Mn_{0.5}$-MOF-74) displayed nearly the same absorption bands as shown in Fig. 5. The typical absorption peak appeared at about 1360 cm^{-1} is related to (C–O) stretching vibration which may be related to the presence of dihydroxyterphthalic acid in MOF.[53] Also, absorption peaks appeared at 1015 and 745 cm^{-1} attributed to γ(C–H), δ(C–H) vibration of aromatic rings.[54] Also, comparing with organic linker, the absorption band that appears at 1633 cm^{-1} that related to stretching vibration of (C=O) group[55] was disappeared or

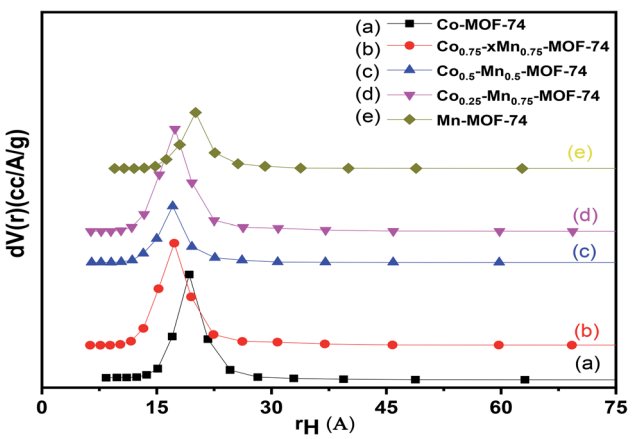

Fig. 4 Pore volume distribution for monometallic and bimetallic MOFs.

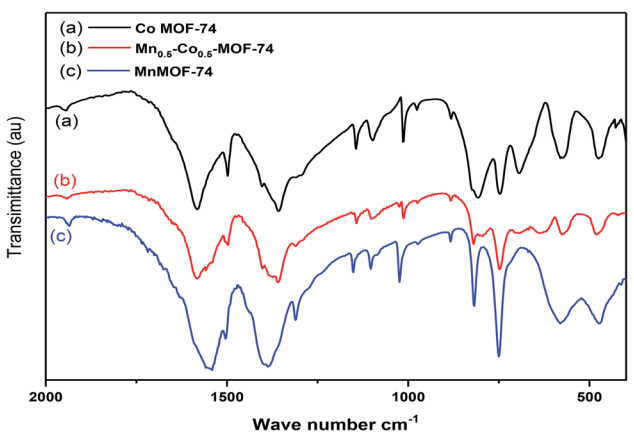

Fig. 5 FTIR spectra of monometallic and bimetallic MOFs.

shifted to lower value at 1547, 1588 and 1577 cm^{-1} for Mn-MOF-74, Co-MOF-74 and $Co_{0.5}$–$Mn_{0.5}$-MOF-74, respectively after addition of metals or bimetals to the linker, which proves that all carboxylic groups of the dihydroxyterphthalic acid are deprotonated and there is no unreacted dihydroxyterphthalic acid on the surface or pores of the prepared MOF-74 (ref. 56) and the desired MOFs were successfully synthesized. Another bands appeared at 1089 and 1140 cm^{-1} related to the hydroxyl groups attached to metal ions (M–OH).[57] In addition, the bands with medium strength appearing at 575 and 476 cm^{-1} were characteristics to Mn–O_{linker} (M = Co or Mn) vibrations. While for $Co_{0.5}$–$Mn_{0.5}$-MOF-74, the absorption band at 582 and 481 cm^{-1} were characteristics to M–O (M = Mn or Co) vibration.[58]

3.4 SEM and EDX analysis

SEM images for monometallic (Co-MOF-74 and Mn-MOF-74) and bimetallic MOF ($Co_{0.5}$–$Mn_{0.5}$-MOF-74) samples were examined by scanning electron microscopy (SEM) and presented in Fig. 6. The images display that all the prepared catalysts exhibit an irregular shape. Also, Fig. 6D display that the Pd nanoparticles were successfully loaded on the surface of $Co_{0.5}$–$Mn_{0.5}$-MOF-74 which were observed as a spots on the MOF composite. These observations were agreed with the XRD results.

For determination the dispersion of Pd, Mn and Co within 2 wt% Pd@$Co_{0.5}$–$Mn_{0.5}$-MOF-74, energy dispersive spectroscopy (EDAX) was performed to map the presence of different metals. The EDAX image displayed that $Co_{0.5}$–$Mn_{0.5}$-MOF-74 was not physical mixture, but Co and Mn were dispersed homogeneously in the sample, also Pd metal were dispersed in the samples as shown in Fig. 7. Fig. 7A displayed that the presence of diffraction peaks related only for Co, Mn, Pd and O elements and the experimental atomic ratio of Co, Mn and Pd element was very close to the theoretical one over 2 wt% Pd@$Co_{0.5}$–$Mn_{0.5}$-MOF-74. All of these data confirm that 2 wt% Pd@$Co_{0.5}$–$Mn_{0.5}$-MOF-74 was successfully synthesized.

3.5 TEM images

The surface morphology of as-prepared monometallic (Co-MOF-74 and Mn-MOF-74) and bimetallic MOF ($Co_{0.5}$–$Mn_{0.5}$-MOF-74) was investigated by transmission electron microscopy (TEM) as displayed in Fig. 8A–C, respectively which are well-consistent with the observed SEM images in terms of dimensionality and morphologies. Fig. 8D–H shows TEM images of 2 wt% Pd@Co-MOF-74 (d), 2 wt% Pd@Mn-MOF-74 (e), 0.5 wt% Pd@$Co_{0.5}$–$Mn_{0.5}$-MOF-74 (f), 2 wt% Pd@$Co_{0.5}$–$Mn_{0.5}$-MOF-74 (g) and 5 wt% Pd@$Co_{0.5}$–$Mn_{0.5}$-MOF-74 (h). It is clear that palladium nanoparticles were homogeneously dispersed over the monometallic and bimetallic MOF.

3.6 Catalytic activity measurement

The results of the catalytic activity of as-prepared Pd supported monometallic (Co-MOF-74 and Mn-MOF-74), bimetallic MOF (Co_x–$Mn_{(1-x)}$-MOF-74) toward CO oxidation were displayed in Fig. 9. As well as, the temperature of 50% (T_{50}) and 100% (T_{100}) conversions were recorded in Table 1. Fig. 2S† and Table 1 compare the catalytic oxidation toward CO oxidation over monometallic and bimetallic MOFs. It's obvious that all these

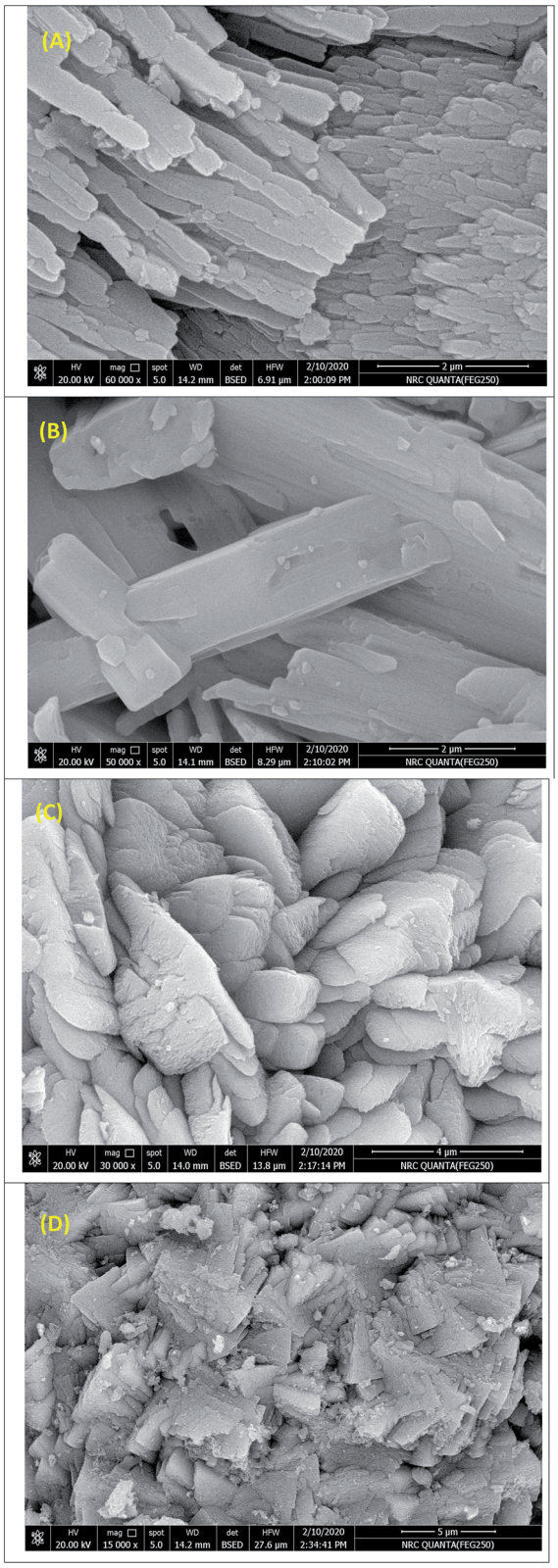

Fig. 6 SEM images for (A) Co-MOF-74, (B) Mn-MOF-74, (C) $Co_{0.5}$–$Mn_{0.5}$-MOF-74 and (D) 2 wt% Pd@$Co_{0.5}$–$Mn_{0.5}$-MOF-74.

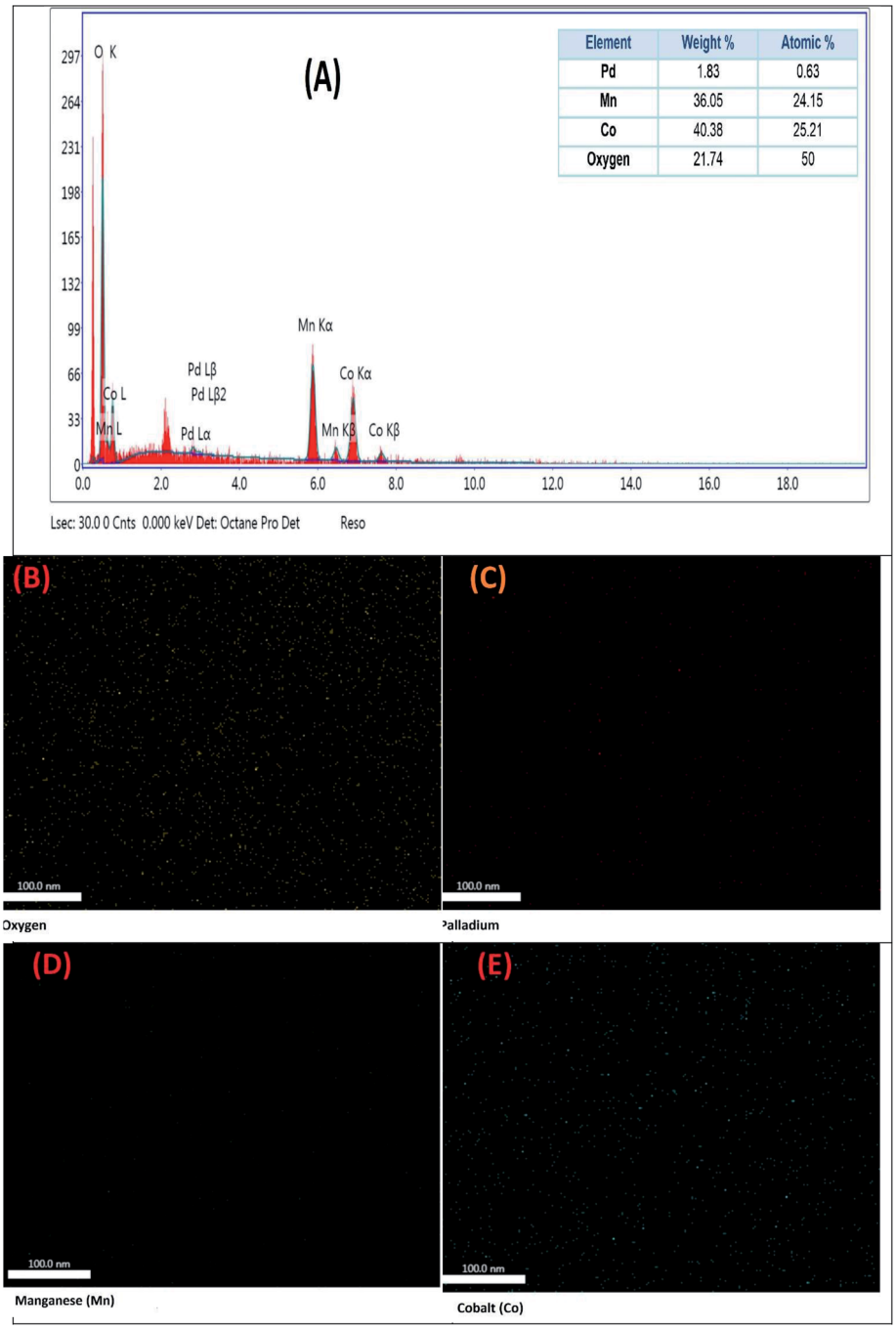

Fig. 7 EDAX mapping of the elements present in 2 wt% Pd@$Co_{0.5}$–$Mn_{0.5}$-MOF-74. (A) EDAX spectra with inset showing elements present. Mapping of (B) oxygen, (C) palladium, (D) manganese and (E) cobalt.

MOFs exhibits catalytic activity after 300 °C which means that the these MOFS have no significant catalytic activity due to Co_x–$Mn_{(1-x)}$-MOF-74 can have decomposed at 300 °C as shown in TGA curves (Fig. 3S†). And the value of $T_{50\%}$ could be related to the MOF oxides not the original MOFs. And the difference in the catalytic activity may be due to the synergetic effect between two metals as oxides.[13] Therefore, developing the synergetic effects between different element (Mn and Co) will be an effective way to promote their related catalytic activities.[59] Secondly, $Co_{0.5}$–$Mn_{0.5}$-MOF-74 has the highest specific surface area which can provide more active sites during the oxidation reaction.[60]

Amazingly, addition of 2 wt% of Pd over monometallic and bimetallic MOFs improve the CO oxidation to a great extent as displays in Fig. 9A. It is clear that the light-off temperature T_{50} and T_{100} of 2 wt% Pd@$Co_{0.5}$–$Mn_{0.5}$-MOF-74 is decreased to 57 and 68 °C as shown in Table 1. Also, CO oxidation conversion for different Pd loadings over $Co_{0.5}$–$Mn_{0.5}$-MOF-74 were examined in Fig. 9B. The Co oxidation conversion was increased

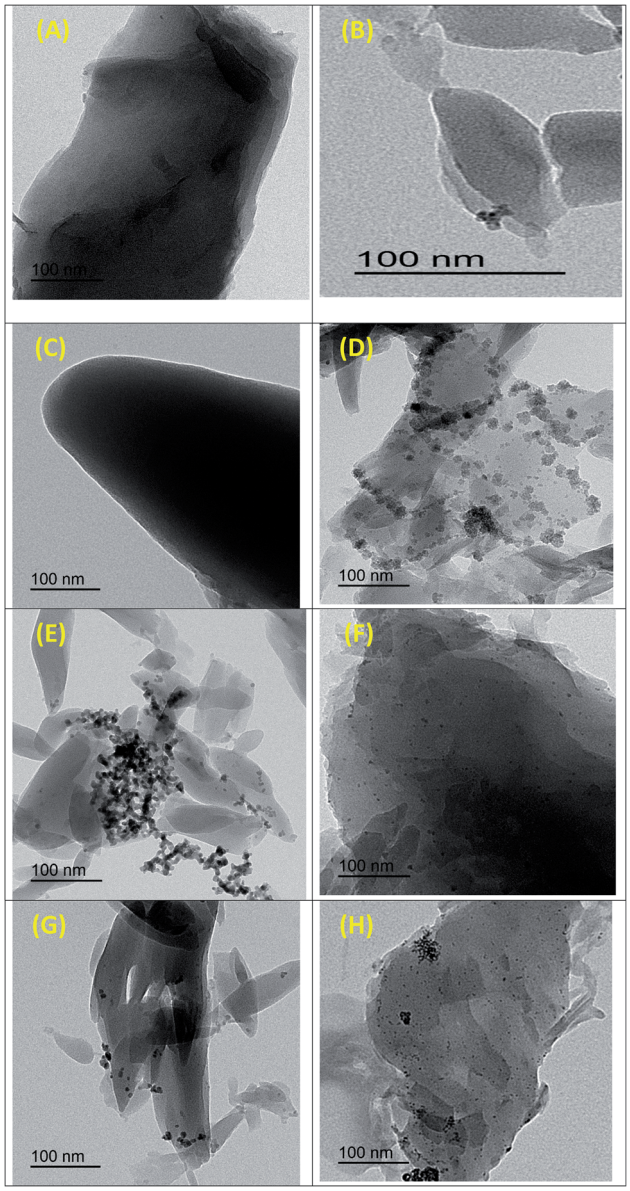

Fig. 8 TEM images of (A) pure Co-MOF-74, (B) pure Mn-MOF-74, (C) $Co_{0.5}$–$Mn_{0.5}$-MOF-74, (D) 2 wt% Pd@Co-MOF-74, (E) 2 wt% Pd@Mn-MOF-74, (F) 0.5 wt% Pd@$Co_{0.5}$–$Mn_{0.5}$-MOF-74, (G) 2 wt% Pd@$Co_{0.5}$–$Mn_{0.5}$-MOF-74 and (H) 5 wt% Pd@$Co_{0.5}$–$Mn_{0.5}$-MOF-74.

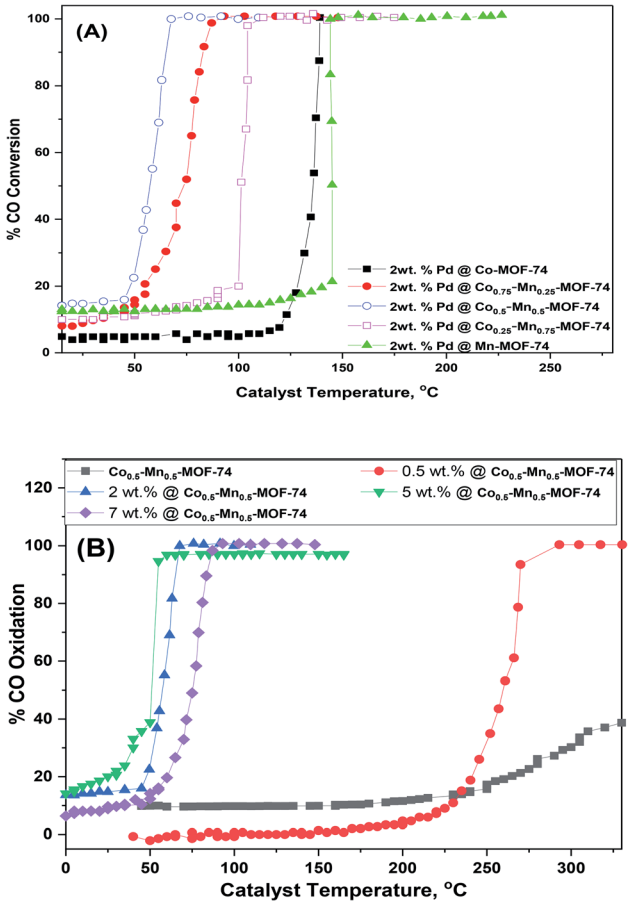

Fig. 9 CO conversion as a function of temperature of (A) 2 wt% Pd supported on the prepared MOFs and (B) different weight% of Pd loaded on $Co_{0.5}$–$Mn_{0.5}$-MOF-74.

sharply as the Pd loadings increased from 0.5 wt%, at which T_{50} and T_{100} conversion occurred at 259 and 290 °C, respectively, to 2 wt%, at which the conversions occurred at 57 and 68 °C, respectively. However, raising the Pd content to 5 wt% slightly decreasing in T_{50} and T_{100} conversion to 50 and 58 °C which is a slight increase in activity when compared to the economic viability of the catalyst. On the other hand, increasing the weight contents of Pd NPs to 7 wt% led to increase in T_{50} and T_{100} conversion to 73 and 84 °C and this may be due to agglomeration of palladium nanoparticles on the support which leads to poor catalytic activity.[61] There are numerous explanations that led to increase the catalytic performance of CO oxidation after addition of Pd nanoparticles. Li and co-workers found that active CO^+ species were formed through the adsorption of CO over Pd^0, then reacts with lattice oxygen to give CO_2 on the interface between Pd and Mn_3O_4 leaving O vacant on the support surface. The O vacant quickly adsorbs oxygen from the gas phase to compensate the support.[62] Also, the highly dispersed Pd nanoparticles over the support and the supportability to supply active oxygen are the most important factors.[63] On the other hand, Hinojosa and co-workers found that PdO adsorbs oxygen to form adsorbed species which are very active in CO oxidation.[64]

Effect of the weight of the catalyst was examined over 2 wt% Pd@$Co_{0.5}$–$Mn_{0.5}$-MOF-74 and displayed in Fig. 10, in which the weight of the catalyst varied from 0.03 g to 0.13 g with constant value of temperature and feed composition. From Fig. 10 and Table 1S,† we found that by increasing the amount of the catalyst from 0.03, 0.06, 0.1 to 0.13, T_{100} conversion of the catalyst was decreased from 228 °C, 126, 68 to 58 °C, respectively. The stability of 5 wt% Pd@$Co_{0.5}$–$Mn_{0.5}$-MOF-74 were also examined, as displayed in Fig. 4S.† In these stability test, the catalyst was kept under continuous stream flow and the other conditions still maintained. The conversion of CO on the catalyst remained stable over 21 hours with a slight decrease in activity. In conclusion, compared with monometallic, bimetallic and Pd nanoparticles supported on these MOFs, 5 wt%

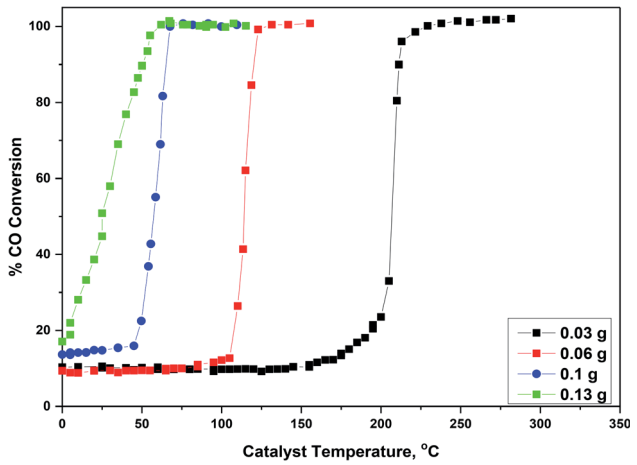

Fig. 10 Effect the weight of the catalyst over 2 wt% Pd@$Co_{0.5}$–$Mn_{0.5}$-MOF-74 on CO conversion.

Pd@$Co_{0.5}$–$Mn_{0.5}$-MOF-74 catalyst shows exceptional activity and stability due to special physicochemical properties.

To further investigate the durability of the as-synthesized catalyst, 5 wt% Pd@$Co_{0.5}$–$Mn_{0.5}$-MOF-74 sample were collected and retested for CO oxidation over six cycle of light-off experiments and the results are shown in Fig. 5S.† The figure displays that the catalyst exhibits good catalytic activity after six runs, indicating the good reusability of the catalyst. The catalytic performance of CO oxidation over Pd nanoparticle catalyst supported on different supports was studied by numerous authors. So, quick comparison studies of the CO oxidation activity over our as-synthesized catalysts with other published Pd supported catalysts[29,31,60,65–67] were shown in Table 2S.† 5 wt% Pd@$Co_{0.5}$–$Mn_{0.5}$-MOF-74 act as effective catalyst in the CO oxidation by achieving the value of 50% and 100% CO conversion at lower temperature.

4. Conclusion

The fabrication of monometallic and bimetallic (Co & Mn) MOFs were successfully synthesized and used as a support for Pd catalysts and then confirmed by different characterization techniques such as XRD, BET, TEM, SEM, EDAX and FT-IR. The as-synthesized catalysts provided sufficient surface area and show a good dispersion of Pd nanoparticles over monometallic and bimetallic MOFs. The prepared catalysts displayed superior catalytic activity for CO oxidation. The Pd contents and the weight of the catalysts could effect on the catalytic activity remarkably. As a result, 5 wt% Pd@$Co_{0.5}$–$Mn_{0.5}$-MOF-74 exhibits the most effective catalyst in the CO oxidation. The difference in catalytic activities of the prepared catalysts may be due to the different contents of Pd nanoparticles. Furthermore, the results displayed an excellent stability of the catalysts during the CO oxidation without a significant decrease in the catalytic performance.

Conflicts of interest

The authors declare that they have no conflict of interest.

References

1 S. Bhattacharjee, C. Chen and W.-S. Ahn, *RSC Adv.*, 2014, **4**, 52500–52525.
2 R. S. Salama, S. A. El-Hakam, S. E. Samra, S. M. El-Dafrawy and A. I. Ahmed, *Int. J. Nano Mater. Sci.*, 2018, **7**, 31–42.
3 S. A. El-Hakam, S. E. Samra, S. M. El-Dafrawy, A. A. Ibrahim, R. S. Salama and A. I. Ahmed, *RSC Adv.*, 2018, **8**, 20517–20533.
4 S. L. James, *Chem. Soc. Rev.*, 2003, **32**, 276–288.
5 R. S. Salama, S. A. El-Hakam, S. E. Samra, S. M. El-Dafrawy and A. I. Ahmed, *Int. J. Mod. Chem.*, 2018, **10**, 195–207.
6 S. Liu, L. Sun, F. Xu, J. Zhang, C. Jiao, F. Li, Z. Li, S. Wang, Z. Wang and X. Jiang, *Energy Environ. Sci.*, 2013, **6**, 818–823.
7 P. Horcajada, C. Serre, G. Maurin, N. A. Ramsahye, F. Balas, M. Vallet-Regi, M. Sebban, F. Taulelle and G. Férey, *J. Am. Chem. Soc.*, 2008, **130**, 6774–6780.
8 J. Zhou, R. Li, X. Fan, Y. Chen, R. Han, W. Li, J. Zheng, B. Wang and X. Li, *Energy Environ. Sci.*, 2014, **7**, 2715–2724.
9 Q. Sun, M. Liu, K. Li, Y. Han, Y. Zuo, F. Chai, C. Song, G. Zhang and X. Guo, *Inorg. Chem. Front.*, 2017, **4**, 144–153.
10 R. Zou, P. Li, Y. Zeng, J. Liu, R. Zhao, H. Duan, Z. Luo, J. Wang, R. Zou and Y. Zhao, *Small*, 2016, **12**, 2334–2343.
11 J. Zhu, Q. Gao and Z. Chen, *Appl. Catal., B*, 2008, **81**, 236–243.
12 J. Yang, B. Du, N. Yuan, X. Jia and J. Li, *New J. Chem.*, 2019, **43**, 6452–6456.
13 X. Qi, H. Tian, X. Dang, Y. Fan, Y. Zhang and H. Zhao, *Anal. Methods*, 2019, **11**, 1111–1124.
14 H. Chen, G. Wei, A. Ispas, S. G. Hickey and A. Eychmüller, *J. Phys. Chem. C*, 2010, **114**, 21976–21981.
15 D. Gupta, D. Dutta, M. Kumar, P. B. Barman, C. K. Sarkar, S. Basu and S. K. Hazra, *Sens. Actuators, B*, 2014, **196**, 215–222.
16 D. Astruc, *Inorg. Chem.*, 2007, **46**, 1884–1894.
17 A. Fihri, M. Bouhrara, B. Nekoueishahraki, J.-M. Basset and V. Polshettiwar, *Chem. Soc. Rev.*, 2011, **40**, 5181–5203.
18 M. Khan, M. Khan, M. Kuniyil, S. F. Adil, A. Al-Warthan, H. Z. Alkhathlan, W. Tremel, M. N. Tahir and M. R. H. Siddiqui, *Dalton Trans.*, 2014, **43**, 9026–9031.
19 S. Sawoo, D. Srimani, P. Dutta, R. Lahiri and A. Sarkar, *Tetrahedron*, 2009, **65**, 4367–4374.
20 A. Dumas and P. Couvreur, *Chem. Sci.*, 2015, **6**, 2153–2157.
21 I. Singh, K. Landfester, A. Chandra and R. Muñoz-Espí, *Nanoscale*, 2015, **7**, 19250–19258.
22 A. Śrębowata, R. Baran, G. Słowik, D. Lisovytskiy and S. Dzwigaj, *Appl. Catal., B*, 2016, **199**, 514–522.
23 S. Hermes, M. Schröter, R. Schmid, L. Khodeir, M. Muhler, A. Tissler, R. W. Fischer and R. A. Fischer, *Angew. Chem., Int. Ed.*, 2005, **44**, 6237–6241.
24 M. Mannaa, H. Altass and R. Salama, *Environ. Nanotechnol. Monit. Manag.*, 2020, **15**, 100410.
25 C. Zlotea, R. Campesi, F. Cuevas, E. Leroy, P. Dibandjo, C. Volkringer, T. Loiseau, G. Férey and M. Latroche, *J. Am. Chem. Soc.*, 2010, **132**, 2991–2997.

26 H. Jiang, Q. Lin, T. Akita, B. Liu, H. Ohashi, H. Oji, T. Honma, T. Takei, M. Haruta and Q. Xu, *Chem.–Eur. J.*, 2011, **17**, 78–81.
27 M. Sabo, A. Henschel, H. Fröde, E. Klemm and S. Kaskel, *J. Mater. Chem.*, 2007, **17**, 3827–3832.
28 S. Kitagawa, R. Kitaura and S. Noro, *Angew. Chem., Int. Ed.*, 2004, **43**, 2334–2375.
29 J. Ye and C. Liu, *Chem. Commun.*, 2011, **47**, 2167–2169.
30 Y. Zhao, C. Zhong and C.-J. Liu, *Catal. Commun.*, 2013, **38**, 74–76.
31 Q. Liang, Z. Zhao, J. Liu, Y.-C. Wei, G.-Y. Jiang and A.-J. Duan, *Acta Phys.-Chim. Sin.*, 2014, **30**, 129–134.
32 T. Gerhardt, M. Göthert, G. Malorny and H. Wilke, *Int. Arch. Arbeitsmed.*, 1971, **28**, 127–140.
33 R. Prasad and P. Singh, *Catal. Rev.*, 2012, **54**, 224–279.
34 S. Royer and D. Duprez, *ChemCatChem*, 2011, **3**, 24–65.
35 J. Qi, K. Zhao, G. Li, Y. Gao, H. Zhao, R. Yu and Z. Tang, *Nanoscale*, 2014, **6**, 4072–4077.
36 A. Xie, J. Guo, W. Liu and Y. Yang, *RSC Adv.*, 2014, **4**, 11357–11359.
37 S. Yang and L. Gao, *J. Am. Chem. Soc.*, 2006, **128**, 9330–9331.
38 S. K. Abd El Rahman, H. M. Altass, M. I. Orif, S. S. Ashour and L. S. Almazroai, *Mater. Res. Bull.*, 2019, **113**, 215–222.
39 M. Morad, M. A. Karim, H. M. Altass and A. E. R. S. Khder, *Environ. Technol.*, 2019, 1–29.
40 H. M. Altass and A. E. R. S. Khder, *Mater. Res. Innovations*, 2018, **22**, 107–114.
41 A. F. Cozzolino, C. K. Brozek, R. D. Palmer, J. Yano, M. Li and M. Dincă, *J. Am. Chem. Soc.*, 2014, **136**, 3334–3337.
42 H. Jiang, C. Wang, H. Wang and M. Zhang, *Mater. Lett.*, 2016, **168**, 17–19.
43 K. Yuan, T. Song, D. Wang, Y. Zou, J. Li, X. Zhang, Z. Tang and W. Hu, *Nanoscale*, 2018, **10**, 1591–1597.
44 I. Strauss, A. Mundstock, M. Treger, K. Lange, S. Hwang, C. Chmelik, P. Rusch, N. C. Bigall, T. Pichler and H. Shiozawa, *ACS Appl. Mater. Interfaces*, 2019, **11**, 14175–14181.
45 H.-Y. Cho, D.-A. Yang, J. Kim, S.-Y. Jeong and W.-S. Ahn, *Catal. Today*, 2012, **185**, 35–40.
46 X. Qin, Y. Sun, N. Wang, Q. Wei, L. Xie, Y. Xie and J.-R. Li, *RSC Adv.*, 2016, **6**, 94177–94183.
47 D. Sun, F. Sun, X. Deng and Z. Li, *Inorg. Chem.*, 2015, **54**, 8639–8643.
48 S. M. El-Dafrawy, R. S. Salama, S. A. El-Hakam and S. E. Samra, *J. Mater. Res. Technol.*, 2020, **9**, 1998–2008.
49 S. Zhao, Y. Wang, J. Dong, C.-T. He, H. Yin, P. An, K. Zhao, X. Zhang, C. Gao and L. Zhang, *Nat. Energy*, 2016, **1**, 1–10.
50 J. Hermannsdörfer and R. Kempe, *Chem.–Eur. J.*, 2011, **17**, 8071–8077.
51 S. M. Hassan, M. A. Mannaa and A. A. Ibrahim, *RSC Adv.*, 2019, **9**, 810–818.
52 A. A. Ibrahim, S. M. Hassan and M. A. Mannaa, *Colloids Surf., A*, 2020, **586**, 124248.
53 R. S. Salama, S. M. Hassan, A. I. Ahmed, W. S. A. El-Yazeed and M. A. Mannaa, *RSC Adv.*, 2020, **10**, 21115–21128.
54 S.-X. Li, Z. Feng-Ying, H. Yang and N. Jian-Cong, *J. Hazard. Mater.*, 2011, **186**, 423–429.
55 Z. Zhang, Z.-Z. Yao, S. Xiang and B. Chen, *Energy Environ. Sci.*, 2014, **7**, 2868–2899.
56 F. Meng, Z. Fang, Z. Li, W. Xu, M. Wang, Y. Liu, J. Zhang, W. Wang, D. Zhao and X. Guo, *J. Mater. Chem. A*, 2013, **1**, 7235–7241.
57 W. S. A. El-Yazeed, Y. G. Abou El-Reash, L. A. Elatwy and A. I. Ahmed, *RSC Adv.*, 2020, **10**, 9693–9703.
58 H. Sun, D. Ren, R. Kong, D. Wang, H. Jiang, J. Tan, D. Wu, S. Chen and B. Shen, *Microporous Mesoporous Mater.*, 2019, **284**, 151–160.
59 W. Tang, W. Li, D. Li, G. Liu, X. Wu and Y. Chen, *Catal. Lett.*, 2014, **144**, 1900–1910.
60 S. K. Abd El Rahman, H. M. A. Hassan, M. A. Betiha, K. S. Khairou and A. A. Ibrahim, *React. Kinet., Mech. Catal.*, 2014, **112**, 61–75.
61 Y. Yan, H. Li, Z. Lu, X. Wang, R. Zhang and G. Feng, *Chin. Chem. Lett.*, 2019, **30**, 1153–1156.
62 G. Li, L. Li, Y. Yuan, J. Shi, Y. Yuan, Y. Li, W. Zhao and J. Shi, *Appl. Catal., B*, 2014, **158**, 341–347.
63 L. Liu, B. Qiao, Y. He, F. Zhou, B. Yang and Y. Deng, *J. Catal.*, 2012, **294**, 29–36.
64 J. A. Hinojosa Jr, H. H. Kan and J. F. Weaver, *J. Phys. Chem. C*, 2008, **112**, 8324–8331.
65 M. Jin, J.-N. Park, J. K. Shon, J. H. Kim, Z. Li, Y.-K. Park and J. M. Kim, *Catal. Today*, 2012, **185**, 183–190.
66 A. Lin, A. A. Ibrahim, P. Arab, H. M. El-Kaderi and M. S. El-Shall, *ACS Appl. Mater. Interfaces*, 2017, **9**, 17961–17968.
67 H. A. Elazab, S. Moussa, B. F. Gupton and M. S. El-Shall, *J. Nanopart. Res.*, 2014, **16**, 2477.